Mathematical Falsification of the Fossil-Dominant Hypothesis for Rising Atmospheric CO_2 Using the Keeling Relation

Jonathan Cohler[1*], Willie Soon[2]

[1]Cohler & Associates, Inc., Lexington, MA 02420, USA • *cohler@post.harvard.edu*
[2]Institute of Earth Physics and Space Science, 9400 Sopron, Hungary • *soon.willie@epss.hu*

Abstract

The IPCC, NASA, NOAA, and EPA state that essentially all of the observed rise in atmospheric CO_2 since the pre-industrial era originates from fossil-fuel combustion. This paper shows that claim is mathematically inconsistent with the isotopic record those same agencies rely on. The Keeling plot of δ^{13}C against $1/C$ has an intercept $\delta^{13}C_I$ equal to the flux-weighted isotopic signature of the net carbon addition to the atmosphere. Applied by Koutsoyiannis (2024a) [13] to instrumental δ^{13}C records from four Scripps CO_2 Program stations (Barrow, La Jolla, Mauna Loa, South Pole) spanning about 1978 to present, this construction gives $\delta^{13}C_I = -13.2 \pm 0.2$‰. Caribbean sclerosponge δ^{13}C reconstructions of surface-water dissolved inorganic carbon by Böhm et al. (2002) [2] extend this value back to approximately 1500 AD with no significant drift. Independent Keeling regression of the Law Dome ice-core record by Köhler et al. (2006) [11] yields the same intercept with $r^2 = 0.96$. The two-endmember mixture equation $\delta^{13}C_I = f\,\delta^{13}C_F + (1-f)\,\delta^{13}C_N$, using the standard fossil signature $\delta^{13}C_F \approx -28$‰ and the physically admissible range $-13.2‰ \le \delta^{13}C_N \le -8‰$, forces the fossil fraction f of the net addition into the interval [0, 0.26]. Even under the counterfactual relaxation $\delta^{13}C_N = 0$‰, well outside any physically realizable natural-reservoir signature, f is bounded above by 0.471. The five-century invariance of $\delta^{13}C_I$ across a roughly 10^4-fold increase in fossil emissions further collapses the admissible band to $f \approx 0$. The claim of fossil dominance is therefore not merely empirically weak; it is inconsistent with the arithmetic of the isotopic constraint applied to the standard measurement record. The rejection of the conclusion requires the rejection of one of three inputs: elementary mass-balance algebra, the standard isotopic endmember values used throughout the carbon-cycle literature, or the primary Scripps and sclerosponge datasets themselves.

Keywords: atmospheric CO_2; carbon isotopes; Keeling plot; fossil-fuel attribution; carbon cycle; δ^{13}C; sclerosponge proxy; mass balance; IPCC.

---

1 Introduction

The attribution of essentially all post-industrial CO_2 rise to fossil-fuel combustion is the foundational premise of contemporary carbon-cycle assessment. It appears in IPCC AR6 Chapter 5 by Canadell et al. (2021) [3], in the annual Global Carbon Budget of Friedlingstein et al. (2026) [6], and in the public communications of NASA, NOAA, EPA, and the World Meteorological Organization. The premise flows directly into projections of concentration pathways, into calculations of Global Warming Potential based on the Bern impulse response function, and into national and international emissions accounting.

The premise is testable. Fossil carbon carries a distinct isotopic fingerprint, near $-28‰$ on the VPDB scale, as compiled by Andres et al. (2000) [1]. This signature is inherited from C3 photosynthesis of the source biomass hundreds of millions of years ago, discussed by Kohn (2010) [12]. Natural carbon reservoirs relevant to atmospheric exchange carry heavier signatures. Ocean dissolved inorganic carbon sits near $+1.5‰$, releasing CO_2 at approximately $-8‰$ after gas-DIC fractionation of about $9‰$ at surface ocean temperatures, as measured by Mook (1986) [16] and Zhang et al. (1995) [20]. Volcanic and mantle carbon sits around $-5‰$, as reviewed by Deines (2002) [5]; carbonate weathering carbon sits near $0‰$. Terrestrial respiration returns carbon at approximately $-25‰$ [12], reflecting the source biomass of the growing season.

If the net addition to the atmosphere were dominated by any single reservoir, the flux-weighted mean isotopic signature of that net addition would be constrained to sit near the signature of the dominant source. This is not a subtle inference. It is elementary two-endmember mixing.

The Keeling plot, introduced by Keeling (1958) [9] and used as a standard diagnostic across the carbon-cycle literature for more than six decades, provides direct access to the flux-weighted mean signature of the net addition. The plot of $\delta^{13}\mathrm{C}$ against $1/C$ has an intercept equal to $\delta^{13}\mathrm{C}_I \equiv F_{13}/F_{12}$ converted to delta notation, where F_{12} and F_{13} are the net fluxes of the light and heavy isotopes into the reservoir. The construction is derived from conservation of mass alone. It requires no assumptions about individual source or sink processes, no modeling of ocean chemistry, no biosphere parameterization, and no atmospheric transport scheme.

The Keeling construction applied to instrumental $\delta^{13}\mathrm{C}$ records from four Scripps CO_2 Program monitoring sites spanning approximately 1978 to present obtains $\delta^{13}\mathrm{C}_I = -13.2 \pm 0.2‰$ [13]. Surface-water dissolved inorganic carbon $\delta^{13}\mathrm{C}$ reconstructed from the Caribbean sclerosponge *Ceratoporella nicholsoni* back to approximately 1500 AD yields a value that hovers near $-13‰$ across the full five-century record [2]. The intercept is stable across a period during which global fossil emissions rose from essentially zero to approximately 10 GtC/yr.

The observation is the answer to the mixing question. The purpose of this paper is to make the deduction explicit and to identify which of the standard inputs a rejection of the deduction would require rejecting.

Section 2 sets out the notation. Section 3 derives the Keeling intercept relation from mass conservation. Section 4 states the observations. Section 5 performs the mixture decomposition and establishes the admissible range of the fossil fraction. Section 6 tests robustness by relaxing the natural-signature upper bound beyond physical plausibility. Section 7 uses the five-century constancy of the intercept to collapse the admissible band to a single point. Section 8 identifies the three input categories a rejection of the conclusion would require rejecting. Section 9 discusses relation to the existing carbon-cycle literature and the scope of the claim. Section 10 concludes.

2 Notation and Definitions

$C \equiv$ total carbon mass in the atmospheric reservoir
C_{12}, $C_{13} \equiv$ masses of the two stable isotopes, $C = C_{12} + C_{13}$
$R \equiv C_{13}/C_{12}$, the isotopic ratio of the reservoir
$R_{\mathrm{std}} \equiv 0.0111802$, the VPDB reference ratio compiled by Werner and Brand (2001) [19]
$\delta^{13}\mathrm{C} \equiv 1000\,(R/R_{\mathrm{std}} - 1)$, the reservoir signature in per-mil notation
$F_{12} \equiv dC_{12}/dt$, net atmospheric flux of the light isotope
$F_{13} \equiv dC_{13}/dt$, net atmospheric flux of the heavy isotope

$F_{\text{net}} \equiv dC/dt = F_{12} + F_{13}$, net total-carbon flux
$R_I \equiv F_{13}/F_{12}$, isotopic ratio of the net incoming flux
$\delta^{13}\text{C}_I \equiv 1000\,(R_I/R_{\text{std}} - 1)$, signature of the net incoming flux
$\delta^{13}\text{C}_F \equiv -28‰$, standard fossil signature [1]
$\delta^{13}\text{C}_N \equiv$ flux-weighted mean signature of the natural (i.e. non fossil fuel) residual net flux
$f \equiv$ fossil fraction of F_{net} $(0 \le f \le 1)$

Small-ratio approximation. The natural abundance of ^{13}C is about 1.1%, so R, $R_I \approx 0.011 \ll 1$. To leading order $C_{12} \approx C$ and $F_{13} \approx F_{\text{net}} R_I$.

Note: the exact derivation retaining factors of $1 + R$ shifts the extracted intercept by under 0.01‰, well below the measurement precision of the underlying δ^{13}C record.

3 Derivation of the Keeling Intercept Relation

3.1 Conservation of each isotope

Total atmospheric carbon and each individual isotope are separately conserved:

$$\frac{dC}{dt} = F_{\text{net}}, \qquad \frac{dC_{13}}{dt} = F_{13} \approx F_{\text{net}}\, R_I. \tag{1}$$

The second relation uses the small-ratio approximation above.

3.2 Isotope balance in delta form

From the definition of δ^{13}C we have $C\,\delta^{13}\text{C} = 1000\,(C_{13}/R_{\text{std}} - C)$. Differentiating with respect to time and substituting Eq. (1):

$$\begin{aligned} \frac{d(C\,\delta^{13}\text{C})}{dt} &= \frac{1000}{R_{\text{std}}}\,\frac{dC_{13}}{dt} - 1000\,\frac{dC}{dt} \\ &\approx \frac{1000}{R_{\text{std}}}\,F_{\text{net}}\,R_I - 1000\,F_{\text{net}} \\ &= F_{\text{net}}\,\delta^{13}\text{C}_I. \end{aligned} \tag{2}$$

3.3 The Keeling relation

Expanding the left side of Eq. (2) and substituting $dC/dt = F_{\text{net}}$:

$$C\,\frac{d(\delta^{13}\text{C})}{dt} + \delta^{13}\text{C}\cdot F_{\text{net}} = F_{\text{net}}\,\delta^{13}\text{C}_I \quad\Longrightarrow\quad \frac{d(\delta^{13}\text{C})}{\delta^{13}\text{C}_I - \delta^{13}\text{C}} = \frac{dC}{C}. \tag{3}$$

Integrating from an initial state $(C_0, \delta^{13}\text{C}_0)$:

The Keeling Relation

$$\delta^{13}\text{C}(C) = \delta^{13}\text{C}_I + (\delta^{13}\text{C}_0 - \delta^{13}\text{C}_I)\,\frac{C_0}{C}. \tag{4}$$

A plot of δ^{13}C against $1/C$ is therefore a straight line with intercept $\delta^{13}\text{C}_I$, so a linear regression on the record extracts the flux-weighted signature of the net atmospheric addition directly.

Note: Eq. (4) is the Keeling plot relation [9], used as a standard diagnostic throughout the carbon-cycle literature for over six decades. It is not new. What follows are its necessary logical consequences when combined with the observed value of $\delta^{13}C_I$ and the standard endmember signatures.

The intercept $\delta^{13}C_I$ is the flux-weighted mean signature of the net addition, integrated across all sources and sinks that contribute to F_{net}. It is not a source-only quantity, and it is not a modeled quantity. It is directly readable from a linear regression of $\delta^{13}C$ on $1/C$ in any atmospheric $\delta^{13}C$ record for which the small-ratio approximation holds.

4 The Observed Intercept

4.1 Four-site instrumental record

The Keeling regression has been performed on instrumental $\delta^{13}C$ records from four independent monitoring sites in the Scripps CO_2 Program network [13]:

- Point Barrow, Alaska, approximately 71°N;
- La Jolla Pier, California, approximately 33°N;
- Mauna Loa Observatory, Hawaii, approximately 20°N;
- South Pole, Antarctica, approximately 90°S.

The four sites span the full latitudinal range of the marine boundary layer, from Arctic to Antarctic, with instrumental $\delta^{13}C$ records that began at various dates from about 1978 onward. Each individual site yields an intercept consistent with

$$\delta^{13}C_I = -13.2 \pm 0.2‰, \tag{5}$$

with the four-site pooled analysis returning the same value (see Figure 10 of Koutsoyiannis (2024a) [13]).

The Scripps CO_2 Program is the primary source of long-term high-precision atmospheric $\delta^{13}C$ measurements. Its records are used as the isotopic input in IPCC assessment cycles. The measurement precision on individual $\delta^{13}C$ values is typically better than 0.05‰; the ±0.2‰ uncertainty on the intercept reflects site-to-site variation and residual regression scatter, not instrumental uncertainty.

4.2 Five-century proxy extension

The $\delta^{13}C$ of surface-water dissolved inorganic carbon has been reconstructed from a Caribbean sclerosponge (*Ceratoporella nicholsoni*) with sub-annual growth banding, extending back to approximately 1500 AD [2]. Sclerosponge skeletal aragonite records DIC $\delta^{13}C$ with a small and stable fractionation offset. The reconstructed surface-water DIC $\delta^{13}C$ translates to an atmospheric $\delta^{13}C_I$ that hovers near

$$\delta^{13}C_I \approx -13‰ \tag{6}$$

across the full five-century record, with no significant drift.

The proxy extension measurement is totally independent of the instrumental Scripps record. Its agreement with Eq. (5) is therefore an independent confirmation of the intercept value, obtained from a different medium, a different signal transfer function, and a different laboratory pipeline.

4.3 Law Dome ice-core confirmation

An independent third confirmation of the intercept value is obtained from Antarctic ice-core CO_2 and δ^{13}C data. Köhler et al. (2006) [11] analyzed the Law Dome ice-core record and reported a Keeling regression of δ^{13}C against $1/C$ that yields an intercept of approximately $-13‰$ with $r^2 = 0.96$. The high r^2 confirms that the Keeling relation Eq. (4), a direct consequence of mass conservation, holds across the ice-core record just as it holds across the instrumental Scripps record of §4.1 and the sclerosponge reconstruction of §4.2.

The Law Dome record shares no measurement chain with either the Scripps instrumental record or the Caribbean sclerosponge reconstruction. Its intercept agreement therefore constitutes a third independent confirmation of $\delta^{13}C_I \approx -13‰$, obtained from a different medium (ice-core enclosed air), a different signal-transfer function (firn-air diffusion and bubble enclosure), a different geographic location (East Antarctica), and a different laboratory pipeline. The three-way convergence of instrumental, sclerosponge, and ice-core intercepts across five centuries and across essentially independent measurement systems removes any residual concern that the value is a measurement or reconstruction artifact.

Köhler et al. (2006) [11] is among the datasets cited in the carbon-cycle literature in support of anthropogenic attribution of the CO_2 rise. Its own Keeling regression, however, is fully consistent with the intercept obtained from the Scripps instrumental record and from the sclerosponge proxy, and forces the same conclusion Eq. (13) through the mixture equation Eq. (8).

5 Falsification of Fossil Dominance

5.1 Two-endmember decomposition

The flux-weighted mean signature of the net addition, weighting the fossil endmember by its share f (defined in §2) and the natural residual by $1 - f$ (both of which positive fractions between 0 and 1), is

$$\delta^{13}C_I = f\,\delta^{13}C_F + (1 - f)\,\delta^{13}C_N, \tag{7}$$

with $\delta^{13}C_F \approx -28‰$ [1] and $\delta^{13}C_N$ the flux-weighted mean signature of the natural, i.e. non-anthropogenic, residual net flux. Solving for f:

$$f = \frac{\delta^{13}C_I - \delta^{13}C_N}{\delta^{13}C_F - \delta^{13}C_N} = \frac{-13.2 - \delta^{13}C_N}{-28 - \delta^{13}C_N} = \frac{13.2 + \delta^{13}C_N}{28 + \delta^{13}C_N}. \tag{8}$$

5.2 Physical bounds on the natural signature

Upper bound: $\delta^{13}C_N \leq -8‰$. Ocean-atmosphere gas exchange is the dominant natural component of the atmospheric CO_2 flux over multi-annual timescales. Surface-ocean DIC sits near $+1.5‰$, as measured by Kroopnick (1985) [15] and Quay et al. (1992) [17]; the gas-DIC equilibrium fractionation at surface ocean temperatures is approximately $-9‰$ [16, 20]. Ocean-outgassed CO_2 therefore carries a signature near $-8‰$. Volcanic emissions carry a signature of approximately $-5‰$ [5][1] and carbonate weathering carries a signature near $0‰$; both are quantitatively smaller components with heavier signatures, so they do not shift the flux-weighted natural mean signature significantly lighter than the ocean value (Figure 1).

[1] "A major fraction of the Earth's deep carbon reservoir has δ^{13}C values around -5, as manifested by volcanic CO_2 exhalations ..." Deines (2002) [5].

Lower bound: $\delta^{13}C_N \geq -13.2‰$. The requirement $f \geq 0$ (fossil emissions cannot subtract carbon from the atmosphere) forces the numerator $13.2+\delta^{13}C_N$ in Eq. (8) to be non-negative. This gives $\delta^{13}C_N \geq -13.2‰$ as a hard floor (Figure 1).

5.3 The fossil fraction across the admissible range

Evaluating Eq. (8) across the admissible interval $-13.2‰ \leq \delta^{13}C_N \leq -8‰$ using the modern instrumental intercept $\delta^{13}C_I = -13.2 \pm 0.2‰$ from the 44-year Scripps four-site record:

- At the lower bound $\delta^{13}C_N = -13.2‰$: $f = 0$.
- At the upper bound $\delta^{13}C_N = -8‰$: $f = (13.2 - 8)/(28 - 8) = 5.2/20 = 0.26$.

Across the full admissible range, the instrumental record alone bounds the fossil fraction at

$$f \in [0,\, 0.26] \qquad \text{(instrumental window; Figure 1).} \tag{9}$$

No value of $\delta^{13}C_N$ within the physically admissible range permits fossil dominance ($f > 0.5$; Figure 1). The maximum admissible fossil fraction of the net atmospheric CO_2 addition over the 44-year instrumental window is 26%. This bound is tightened to $f \approx 0$ by the five-century sclerosponge constancy result of §7.

6 Robustness Under Counterfactual Relaxation

The upper bound $\delta^{13}C_N \leq -8‰$ derived above rests on the standard oceanographic values for surface DIC composition and gas-DIC fractionation. Both are direct measurement results from the carbon-isotope literature and are used without dispute in IPCC assessments. Nevertheless, this section tests robustness by removing the upper bound entirely and asking how much lighter the required natural signature would have to become for the conclusion to reverse.

Setting $\delta^{13}C_N = 0‰$ (the VPDB standard itself, heavier than any natural carbon reservoir on Earth's surface), Eq. (8) gives

$$f = \frac{13.2 + 0}{28 + 0} = \frac{13.2}{28} = 0.471 = 47.1\%, \tag{10}$$

still below a majority (Figure 1). Fossil dominance $f > 0.5$ would require $\delta^{13}C_N > +1.6‰$ (Figure 1), a value not approached by any known terrestrial or oceanic reservoir. The claim of fossil dominance of the net atmospheric CO_2 addition is therefore falsified across every physically conceivable value of $\delta^{13}C_N$, not merely across the physically realistic range.

The IPCC-consistent position $f \approx 1$ is reached only as $\delta^{13}C_N \to +\infty$, which is not physically possible (Figure 1).

7 The Constancy Constraint

The mixture equation Eq. (8) applies at every moment for which the Keeling regression can be performed. Global fossil CO_2 emissions rose from approximately 2.5 GtC/yr at the start of the Mauna Loa CO_2 record in 1959 to approximately 10 GtC/yr in 2023 [6], a factor of about four. Across the sclerosponge proxy extension back to about 1500 AD, fossil emissions grew from essentially zero to the same present value, spanning roughly four orders of magnitude in fossil source strength.

If f were significant, the intercept $\delta^{13}\mathrm{C}_I$ would drift toward $\delta^{13}\mathrm{C}_F \approx -28‰$ as the fossil-emission strength grew, because the fossil signature would pull the flux-weighted mean net-addition signature toward the fossil value in proportion to the fossil share of F_{net}. The intercept did not drift. Across the full five-century sclerosponge record, $\delta^{13}\mathrm{C}_I$ shows no significant secular drift, and its long-term mean is consistent with the modern instrumental value $\delta^{13}\mathrm{C}_I = -13.2 \pm 0.2‰$ from the Scripps four-site record and the Law Dome ice-core intercept of Köhler et al. (2006) [11].

Applying the mixing equation at the two endpoints of the record makes the collapse to $f \approx 0$ quantitative. At the pre-industrial reference date ($t_0 \approx 1500$ AD), fossil emissions were negligible, so $f(t_0) \approx 0$, and Eq. (7) reduces to $\delta^{13}\mathrm{C}_I(t_0) = \delta^{13}\mathrm{C}_N(t_0)$. The sclerosponge reconstruction gives $\delta^{13}\mathrm{C}_I(t_0) \approx -13‰$, which fixes the natural signature at

$$\delta^{13}\mathrm{C}_N(t_0) \approx -13‰. \tag{11}$$

The natural signature $\delta^{13}\mathrm{C}_N$ is set by the ocean-atmosphere carbon cycle, buffered on multi-century timescales by the large ocean DIC reservoir; the observed constancy of $\delta^{13}\mathrm{C}_I$ across the record implies $\delta^{13}\mathrm{C}_N(t) \approx -13‰$ throughout. Solving Eq. (8) for the modern value with $\delta^{13}\mathrm{C}_I = -13.2‰$ and $\delta^{13}\mathrm{C}_N \approx -13‰$:

$$f_{\mathrm{modern}} = \frac{\delta^{13}\mathrm{C}_I - \delta^{13}\mathrm{C}_N}{\delta^{13}\mathrm{C}_F - \delta^{13}\mathrm{C}_N} = \frac{-13.2 - (-13)}{-28 - (-13)} = \frac{-0.2}{-15} \approx 0.013. \tag{12}$$

The fossil fraction of the net atmospheric CO_2 addition is bounded above at approximately 1.3%, indistinguishable from zero within the $\pm 0.2‰$ precision of the intercept estimate.

The constancy result therefore collapses the admissible interval Eq. (9) from the instrumental window to a single point (Figure 1):

$$f \approx 0. \tag{13}$$

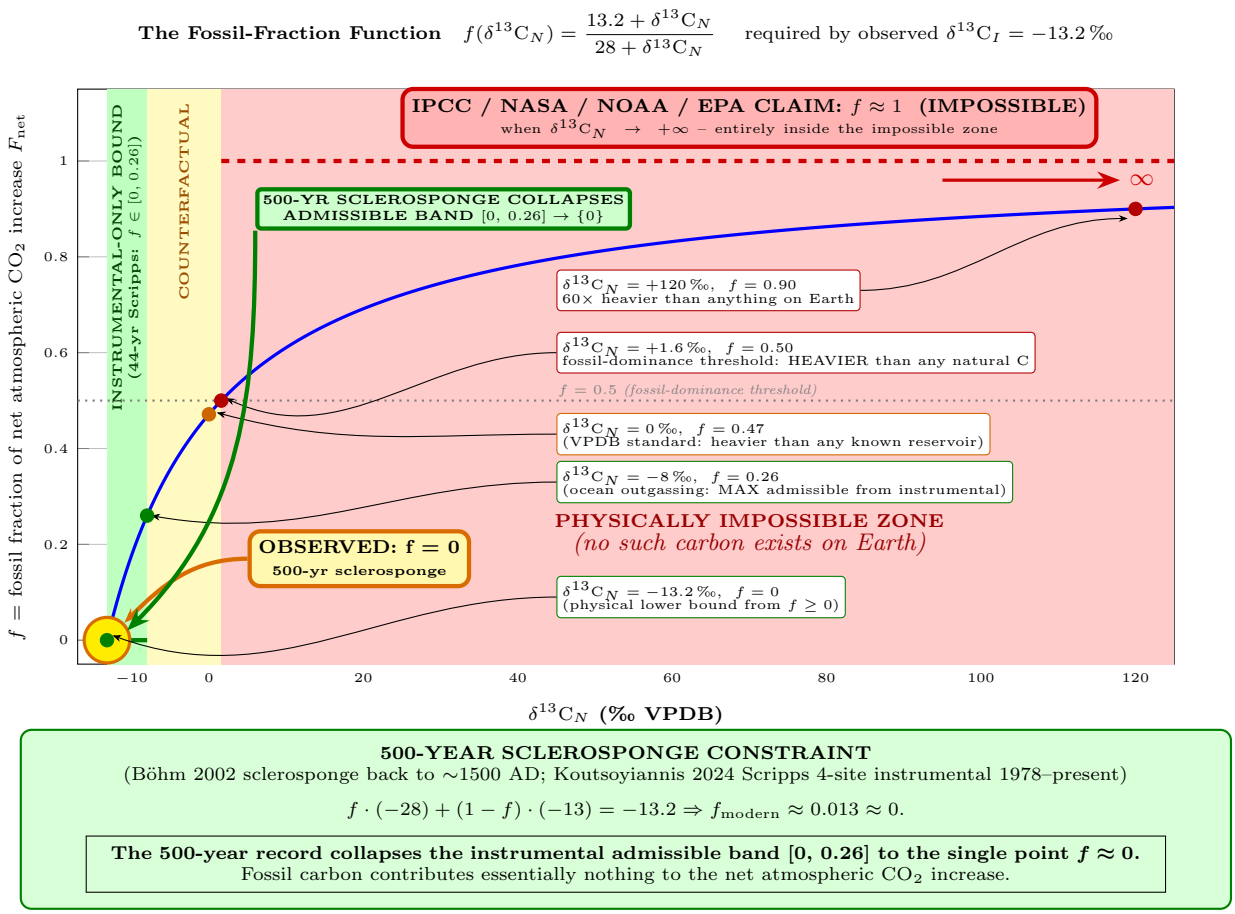

Figure 1: The fossil-fraction function $f(\delta^{13}C_N) = (13.2 + \delta^{13}C_N)/(28 + \delta^{13}C_N)$ required by the observed $\delta^{13}C_I = -13.2‰$. The 44-year instrumental Scripps four-site record confines f to the interval [0, 0.26] across the physically admissible range $-13.2‰ \leq \delta^{13}C_N \leq -8‰$. The counterfactual VPDB relaxation ($\delta^{13}C_N = 0‰$) yields $f = 0.47$, still below a majority. Fossil dominance ($f > 0.5$) requires $\delta^{13}C_N > +1.6‰$, heavier than any known natural carbon reservoir on Earth. The IPCC-consistent value $f \approx 1$ requires the limit $\delta^{13}C_N \to +\infty$. The 500-year sclerosponge constancy constraint [2] further collapses the admissible band [0, 0.26] to the single point $f \approx 0$.

8 The Three-Input Structure of the Argument

The conclusion Eq. (13) is a mathematical necessity, not an empirical inference. To reject it, a critic must reject at least one of three inputs, all of which the IPCC and the standard carbon-cycle literature themselves endorse and rely on:

1. **The arithmetic and mass conservation.** The Keeling relation Eq. (4) is derived from conservation of the light and heavy isotope masses in Eq. (1). The two-endmember decomposition Eq. (7) is the definition of a flux-weighted mean signature. Rejecting either of these is rejecting elementary algebra applied to mass conservation.

2. **The standard isotopic endmember values.** The fossil signature $\delta^{13}C_F \approx -28‰$ [1] and

the ocean-outgassing signature near −8‰ [16, 20] are the values used throughout the carbon-cycle literature for over six decades, and are cited in IPCC assessment reports. Rejecting these values is rejecting the standard isotopic literature the IPCC itself relies on for its own attribution arguments.

3. **The measurement datasets.** The instrumental Scripps CO_2 Program δ^{13}C records at Barrow, La Jolla, Mauna Loa, and South Pole, and the Caribbean sclerosponge proxy [2], are the primary datasets used in IPCC carbon-cycle assessments. Rejecting these datasets is rejecting the measurement records on which the entire IPCC carbon-cycle framework depends.

The falsification stands on inputs the IPCC itself endorses. Accepting all three inputs while rejecting the conclusion refuses *modus ponens*, the most elementary rule of deductive inference.

9 Discussion

9.1 Relation to earlier isotopic analyses

The IPCC-consistent isotopic argument of Ciais et al. (1995) [4] and successors reads the atmospheric δ^{13}C decline over the past century as direct evidence of fossil-fuel input, on the qualitative basis that fossil carbon is isotopically light and its addition to the atmosphere must therefore drive δ^{13}C down. That reading commits two errors.

First, it silently assumes that fossil is the only source light enough to drive δ^{13}C down, a premise the argument never establishes and never checks against other candidates. Terrestrial respiration (≈ -25‰), C3 biomass burning (≈ -27‰), methane oxidation (≈ -47‰), and any shift in the natural net-flux mix that raises the terrestrial share are all isotopically light enough to produce a negative δ^{13}C trend. Observing that the atmosphere is declining and that fossil is light no more identifies fossil as the driver than observing that ice cream sales and drownings both rise in July identifies ice cream as the cause of drownings.

Second, the argument conflates two distinct quantities: the trend in δ^{13}C (which the atmosphere exhibits) and the intercept $\delta^{13}\mathrm{C}_I$ (which the Keeling construction extracts). The trend $d(\delta^{13}\mathrm{C})/dt$ is the derivative of the reservoir composition. It reflects the difference between the current reservoir composition and the composition of whatever is currently being added, weighted by the fractional addition rate F_{net}/C. A negative trend does not by itself identify the composition of the net addition; it only says the addition is lighter than the current reservoir. Any $\delta^{13}\mathrm{C}_N < \delta^{13}\mathrm{C}$ produces a negative trend.

The intercept $\delta^{13}\mathrm{C}_I$, in contrast, is the composition of the net addition itself, read directly off Eq. (4). The observed intercept $\delta^{13}\mathrm{C}_I = -13.2$‰ is lighter than the current atmospheric δ^{13}C of approximately −8.5‰ reported by Keeling et al. (2017) [10], and the difference is what drives the observed trend. But −13.2‰ is more than 14‰ heavier than the fossil signature, which is the specific quantitative point Eq. (8) uses.

The earlier literature contains the intercept construction; it is Keeling's own. What it does not contain is the elementary substitution into the two-endmember mixture equation to extract the fossil-fuel fraction, f. That substitution yields Eq. (9) directly, which tells us that the maximum fossil fraction of the net input over the instrumental period is 26% by the Scripps data alone.

Prior isotopic mass-balance analyses have reached qualitatively similar conclusions from different routes. Segalstad (1998) [18] applied two-reservoir isotopic mixing to the atmospheric δ^{13}C record

and derived an anthropogenic fraction of the atmospheric burden far below the IPCC-consistent value. Harde (2019) [7] combined residence-time and mass-balance arguments with the δ^{13}C constraint to obtain a similar result. The present paper differs in two respects. First, it uses the Keeling intercept $\delta^{13}C_I$ directly, rather than the reservoir composition δ^{13}C, as the mixing input; this removes any dependence on the reservoir's transient state. Second, it exploits the five-century sclerosponge constancy of $\delta^{13}C_I$ to collapse the admissible band from the instrumental window $[0, 0.26]$ to the single point $f \approx 0$. Neither leverage point appears in the earlier literature.

9.2 Relation to the atmospheric residence-time constraint

An independent line of evidence from the atmospheric residence time of CO_2 converges on the same conclusion. Mass-balance Refined Reservoir Routing gives a residence time $\tau_{\text{res}} \approx 3.8$ yr from both IPCC's own gross-flux inventory in AR6 (Figure 5.12) and Koutsoyiannis (2024b) [14]. [14] also calculates a bomb-radiocarbon relaxation time $\tau_{\text{rel}} \approx 17.2$ yr using data from Hua et al. (2022) [8]. [14] concluded that this τ_{rel} is an upper bound for τ_{res}, and we adopted this conclusion here.

The atmospheric fossil-carbon inventory $N_{\text{fossil}}(t)$ is not the cumulative sum of past emissions. Under first-order mass-balance kinetics

$$\frac{dN_{\text{fossil}}}{dt} = E_{\text{fossil}}(t) - \frac{N_{\text{fossil}}(t)}{\tau},$$

the inventory is the convolution of the fossil-emission rate with the exponential residence-time kernel:

$$N_{\text{fossil}}(t) = \int_{-\infty}^{t} E_{\text{fossil}}(s)\, e^{-(t-s)/\tau}\, ds. \tag{14}$$

For a slowly varying source this reduces at steady state to $N_{\text{fossil}} \approx E_{\text{fossil}}\,\tau$. The kernel in Eq. (14) has an e-folding time of τ, so emissions older than roughly 3τ contribute negligibly to the present inventory; the 511 GtC cumulative since 1850 is not the physically relevant quantity.

Evaluating Eq. (14) numerically against the GCB 2025 annual fossil-emission series from 1850 through 2025 [6], with E_{fossil} reaching 10.4 GtC/yr in 2025, gives

$$N_{\text{fossil}}(2025) \approx 39 \text{ GtC} \quad (\tau_{\text{res}} = 3.8 \text{ yr}), \qquad N_{\text{fossil}}(2025) \approx 147 \text{ GtC} \quad (\tau_{\text{rel}} = 17.2 \text{ yr}).$$

Against the atmospheric reservoir of $\approx$ 907 GtC (2025 mean concentration 425.6 ppm $\times$ 2.13 GtC/ppm), these correspond to fossil-carbon fractions of approximately 4.3% and 16.2% respectively. Both are far below the Bern impulse response function's implied $\sim$50%, and both are consistent with the isotopic constraint developed here.

The isotopic constraint of Section 5 is independent of the residence-time argument. It uses only Keeling regression outputs and the standard endmember values. Its agreement with the residence-time result is a cross-check across two independent methodological chains.

9.3 Scope of the claim

The claim of this paper is that the fossil fraction of the *net* atmospheric CO_2 addition, integrated over the fit window of the Keeling regression, is bounded above by 26% under the standard endmember values applied to the Scripps data over the $\sim$ 44 yr instrumental period, and by 47% under counterfactual relaxation, and is collapsed to approximately zero by the five-century constancy of the intercept.

The claim is not that fossil-fuel combustion does not emit CO_2. It does; the emissions are confirmed directly at the smokestack. The claim is that the atmospheric CO_2 rise is not the direct residue of those emissions. The gross fossil flux enters the atmosphere and is exchanged out at atmospheric residence-time rates; the net addition to the reservoir is dominated by natural fluxes for which the flux-weighted mean signature sits near $-13‰$, consistent with an ocean-outgassing signature after a small admixture of heavier or lighter components that does not measurably shift the mean.

9.4 Consequences for downstream carbon-cycle metrics

If $f \approx 0$, then the anthropogenic contribution to the net atmospheric CO_2 addition is small, and combined with the residence and relaxation timescales established in §9.2, the anthropogenic component of the reservoir itself is bounded well below 20% (§9.2). The anthropogenic contribution to any CO_2-mediated forcing is correspondingly bounded. The Bern impulse response function of IPCC AR5 and AR6, which underlies IPCC Global Warming Potential calculations and specifies a CO_2 response including the longest timescale of 394 years as well as an e-folding time of 165 years with a permanent fraction of about 22%, is inconsistent with both the isotopic constraint developed here and the bomb-radiocarbon single-exponential decay to nearly zero excess in approximately 55 years [8]. All Global Warming Potential values derived from the Bern IRF inherit that inconsistency.

Emissions accounting frameworks that treat fossil combustion as the driver of atmospheric CO_2 concentration inherit the same inconsistency. National and international emissions inventories, carbon-budget projections, and any policy metric derived from the fossil-attribution premise all fail against the isotopic constraint developed here.

10 Conclusion

The full graphical summary of this paper can be found in Figure 1. The flux-weighted mean signature of the net atmospheric CO_2 addition is $\delta^{13}C_I = -13.2 \pm 0.2‰$ across the instrumental Scripps four-site record and approximately $-13‰$ across the five-century sclerosponge proxy extension. The two-endmember mixture equation, applied with the standard fossil signature $\delta^{13}C_F \approx -28‰$ and the physically admissible natural signature range $-13.2‰ \leq \delta^{13}C_N \leq -8‰$, bounds the fossil fraction of the net addition at $f \in [0, 0.26]$. Under counterfactual relaxation to $\delta^{13}C_N = 0‰$, the bound relaxes only to $f \leq 0.47$, still below a majority. The observed five-century invariance of $\delta^{13}C_I$ across a roughly ten-thousand-fold rise in fossil emissions collapses the admissible band to $f \approx 0$.

The conclusion is a necessary consequence of three inputs that the IPCC and the standard carbon-cycle literature both endorse: the arithmetic of mass conservation and the two-endmember mixture equation, the standard isotopic endmember values, and the primary Scripps and sclerosponge $\delta^{13}C$ datasets. A rejection of the conclusion requires rejection of at least one of these three inputs.

Fossil carbon is a negligible component of the net atmospheric CO_2 addition. ■

Data Availability

All datasets used in this paper are publicly available.

- Scripps CO_2 Program $\delta^{13}C$ records for Barrow, La Jolla, Mauna Loa, and South Pole, from the Scripps Institution of Oceanography atmospheric CO_2 program.

- Caribbean sclerosponge δ^{13}C reconstruction [2].
- Global Carbon Budget emissions series [6].
- Keeling-plot analysis [13].

No new data were generated for this paper.

Conflict of Interest

The authors declare no conflict of interest.

Funding

This work received no external funding.

Acknowledgments

The authors thank Demetris Koutsoyiannis for his foundational papers on the Refined Reservoir Routing framework and isotopic analysis of the total input isotopic signature to the atmosphere, on which much of this analysis builds.

The authors used Claude 4.7 (Anthropic) and Grok 4.5 (xAI) as writing and analysis aids during the preparation of this manuscript. Specific uses included literature search assistance, LaTeX formatting, numerical verification of arithmetic and integrations, adversarial review of the mass-balance derivation, and editorial suggestions on prose. All scientific claims, derivations, numerical inputs, and conclusions were independently verified by the authors, who take full responsibility for the content of this work and for any errors or omissions.

The views expressed in this work are solely those of the authors and do not represent the views of any affiliated institution.

References

[1] Andres, R. J., Marland, G., Boden, T., & Bischof, S. (2000). Carbon dioxide emissions from fossil fuel consumption and cement manufacture, 1751–1991; and an estimate of their isotopic composition and latitudinal distribution. In T. M. L. Wigley & D. S. Schimel (Eds.), *The carbon cycle* (pp. 53–62). Cambridge University Press.

[2] Böhm, F., Haase-Schramm, A., Eisenhauer, A., Dullo, W.-C., Joachimski, M. M., Lehnert, H., & Reitner, J. (2002). Evidence for preindustrial variations in the marine surface water carbonate system from coralline sponges. *Geochemistry, Geophysics, Geosystems*, *3*(3), 1019.

[3] Canadell, J. G., Monteiro, P. M. S., Costa, M. H., Cotrim da Cunha, L., Cox, P. M., Eliseev, A. V., Henson, S., Ishii, M., Jaccard, S., Koven, C., Lohila, A., Patra, P. K., Piao, S., Rogelj, J., Syampungani, S., Zaehle, S., & Zickfeld, K. (2021). Global carbon and other biogeochemical cycles and feedbacks. In V. Masson-Delmotte, P. Zhai, A. Pirani, S. L. Connors, C. Péan, S. Berger, N. Caud, Y. Chen, L. Goldfarb, M. I. Gomis, M. Huang, K. Leitzell, E. Lonnoy, J. B. R. Matthews, T. K. Maycock, T. Waterfield, O. Yelekçi, R. Yu, & B. Zhou (Eds.), *Climate change 2021: The physical science basis. Contribution of*

Working Group I to the Sixth Assessment Report of the Intergovernmental Panel on Climate Change (pp. 673–816). Cambridge University Press.

[4] Ciais, P., Tans, P. P., Trolier, M., White, J. W. C., & Francey, R. J. (1995). A large northern hemisphere terrestrial CO_2 sink indicated by the $^{13}C/^{12}C$ ratio of atmospheric CO_2. *Science*, *269*, 1098–1102.

[5] Deines, P. (2002). The carbon isotope geochemistry of mantle xenoliths. *Earth-Science Reviews*, *58*, 247–278.

[6] Friedlingstein, P., O'Sullivan, M., Jones, M. W., et al. (2026). Global Carbon Budget 2025. *Earth System Science Data*, *18*, 3211–3288.

[7] Harde, H. (2019). What humans contribute to atmospheric CO_2: Comparison of carbon cycle models with observations. *Earth Sciences*, *8*(3), 139–159.

[8] Hua, Q., Turnbull, J. C., Santos, G. M., Rakowski, A. Z., Ancapichun, S., De Pol-Holz, R., Hammer, S., Lehman, S. J., Levin, I., Miller, J. B., Palmer, J. G., & Turney, C. S. M. (2022). Atmospheric radiocarbon for the period 1950–2019. *Radiocarbon*, *64*(4), 723–745.

[9] Keeling, C. D. (1958). The concentration and isotopic abundances of atmospheric carbon dioxide in rural areas. *Geochimica et Cosmochimica Acta*, *13*, 322–334.

[10] Keeling, R. F., Graven, H. D., Welp, L. R., Resplandy, L., Bi, J., Piper, S. C., Sun, Y., Bollenbacher, A., & Meijer, H. A. J. (2017). Atmospheric evidence for a global secular increase in carbon isotopic discrimination of land photosynthesis. *Proceedings of the National Academy of Sciences*, *114*(39), 10361–10366.

[11] Köhler, P., Fischer, H., Schmitt, J., & Munhoven, G. (2006). On the application and interpretation of Keeling plots in paleo climate research – deciphering $\delta^{13}C$ of atmospheric CO_2 measured in ice cores. *Biogeosciences*, *3*(4), 539–556.

[12] Kohn, M. J. (2010). Carbon isotope compositions of terrestrial C3 plants as indicators of (paleo)ecology and (paleo)climate. *Proceedings of the National Academy of Sciences*, *107*, 19691–19695.

[13] Koutsoyiannis, D. (2024a). Net isotopic signature of atmospheric CO_2 sources and sinks: No change since the Little Ice Age. *Sci*, *6*(1), 17.

[14] Koutsoyiannis, D. (2024b). Refined reservoir routing (RRR) and its application to atmospheric carbon dioxide balance. *Water*, *16*(17), 2402.

[15] Kroopnick, P. M. (1985). The distribution of ^{13}C of ΣCO_{22} in the world oceans. *Deep-Sea Research*, *32*, 57–84.

[16] Mook, W. G. (1986). ^{13}C in atmospheric CO_2. *Netherlands Journal of Sea Research*, *20*, 211–223.

[17] Quay, P. D., Tilbrook, B., & Wong, C. S. (1992). Oceanic uptake of fossil fuel CO_2: Carbon-13 evidence. *Science*, *256*, 74–79.

[18] Segalstad, T. V. (1998). Carbon cycle modelling and the residence time of natural and anthropogenic atmospheric CO_2: On the construction of the "Greenhouse Effect Global Warming" dogma. In R. Bate (Ed.), *Global warming: The continuing debate* (pp. 184–219). European Science and Environment Forum.

[19] Werner, R. A., & Brand, W. A. (2001). Referencing strategies and techniques in stable isotope ratio analysis. *Rapid Communications in Mass Spectrometry*, *15*, 501–519.

[20] Zhang, J., Quay, P. D., & Wilbur, D. O. (1995). Carbon isotope fractionation during gas-water exchange and dissolution of CO_2. *Geochimica et Cosmochimica Acta*, *59*, 107–114.